RSC Advances

PAPER

View Article Online
View Journal | View Issue

Cite this: *RSC Adv.*, 2026, **16**, 14123

Wet-spun Ag/PZT/TPU composite piezoelectric fibers with ultrahigh flexibility: fabrication, performance, and sensing response

Wanwan Liu, *[ab] Huabin Li,[b] Jingjing Xu,[c] Shuangquan Wu[c] and Zhidong Chen*[a]

In the field of self-powered sensing, the demand for materials with enhanced wearing comfort and superior flexibility has become increasingly prominent, driven by the rapid advancement of wearable electronics and intelligent monitoring technologies. Although piezoelectric ceramics exhibit exceptional piezoelectric performance, their inherent brittleness and poor deformability severely restrict their practical applicability in flexible self-powered sensors. In pursuit of addressing the requirement for improved wearing comfort while retaining efficient energy conversion capability, elastomer-based composite fibers have emerged as a promising class of materials and developed rapidly in recent years. Nevertheless, a critical challenge remains in achieving uniform dispersion of fillers within the polymer matrix and the fabrication of defect-free composite fibers under high filler loading, primarily due to the significant surface energy discrepancy between the fillers and the polymer matrix. In this work, a novel thermoplastic polyurethane (TPU) based composite piezoelectric fiber with strong organic–inorganic interfacial adhesion and uniform high-content filler dispersion was proposed, achieved by interfacial modification of PZT and *in situ* reduced Ag nanoparticles (AgNPs) into TPU *via* wet spinning for flexible wearable piezoelectric sensors. Notably, even at total inorganic filler loadings surpassing 80 wt%, the resultant composite fibers maintain outstanding mechanical properties, with breaking strength >10 MPa and elongation at break >200%. When optimized with 80 wt% PZT and 3 wt% Ag precursor, the composite fibers, after weaving into fabrics and corona polarization, exhibit ultrahigh piezoelectric output sensitivity of 133 ± 2.1 mV N^{-1} and ultrafast response time (≈20 ms). This work offers a scalable fabrication route for high-performance piezoelectric fibers, which is helpful for self-powered sensors with better performance and more comfortable use in human motion monitoring and recognition.

Received 23rd December 2025
Accepted 9th March 2026

DOI: 10.1039/d5ra09925k

rsc.li/rsc-advances

1 Introduction

Piezoelectric sensors have emerged as one of the core devices in the intelligent sensing field, leveraging their advantages of direct mechanical-to-electrical energy conversion, self-powered capability, millisecond-level dynamic response speed, and no need for external power supply.[1–3] Their application scenarios have expanded from traditional industrial detection to cutting-edge fields, including smart wearable devices (*e.g.*, wristbands for motion posture monitoring),[4,5] medical monitoring (*e.g.*, patches for pulse waveform acquisition),[6,7] human–computer interaction (*e.g.*, flexible touch gloves),[8,9] and bionic electronics (*e.g.*, cochlear implants).[10,11]

Generally, piezoelectric materials can be categorized into three types: inorganic piezoelectric ceramics (*e.g.*, lead zirconate titanate (PZT), barium titanate ($BaTiO_3$)), organic piezoelectric polymers (*e.g.*, poly(vinylidene fluoride) (PVDF) and its copolymers), and composite piezoelectric materials. Among them, PZT exhibits an ultrahigh piezoelectric coefficient of 500–600 pC N^{-1}, making it the inorganic material with the most outstanding piezoelectric performance to date.[12,13] However, its inherent drawbacks of high brittleness (elongation at break <1%) and poor processability limit its application in flexible devices. Although $BaTiO_3$ features a relatively low cost and greater environmental benignity, its relatively low Curie temperature (≈120 °C) renders it prone to depolarization and subsequent functional failure during service. Organic piezoelectric polymers, represented by fluorine-containing copolymers, possess excellent flexibility and biocompatibility, but their piezoelectric coefficient is merely 20–60 pC N^{-1}, leading to insufficient energy conversion efficiency.[14–16] Composite piezoelectric materials achieve performance complementarity by dispersing inorganic piezoelectric phases within a flexible polymer matrix. Thermoplastic polyurethane (TPU) has emerged as an ideal flexible matrix due to its integrated

[a]*School of Materials Science and Engineering, Changzhou University, Changzhou, Jiangsu, China. E-mail: chen@cczu.edu.cn*

[b]*School of Textile and Clothing, Nantong University, Nantong, Jiangsu, China. E-mail: liuww@ntu.edu.cn*

[c]*Kuangda Technology Group Co., Ltd, Changzhou, Jiangsu, China*

advantages of high elasticity (elongation at break >500%), wear resistance, and hydrolysis resistance.[17–19]

Nevertheless, a prominent contradiction exists in this composite system: to achieve a detectable piezoelectric response, the mass fraction of PZT typically needs to be increased to over 60% (even up to 80% in some studies).[20,21] However, high PZT content results in increased spinning difficulty and more internal structural defects of the composite system, leading to a dilemma where piezoelectric performance and flexibility are mutually exclusive. Fortunately, researchers have found that incorporating conductive materials, such as incorporating conductive fillers (*e.g.*, silver nanoparticles (AgNPs), carbon nanomaterials, MXenes) into the piezoelectric polymer/ceramic matrix or constructing core–shell structured piezoelectric ceramics into the composite system can modulate the dielectric constant of the composite.[22–24] This implies that under the premise of ensuring equivalent piezoelectric output, the PZT loading can be appropriately reduced, thereby alleviating the constraint of high ceramic content on the processability of the composite fibers. The enhancement of piezoelectric performance is governed by the synergistic interplay of three distinct roles played by conductive fillers: the facilitation of dipole alignment during poling treatment, the augmentation of electromechanical conversion efficiency upon stress transfer, and the establishment of expedited charge transport pathways during energy harvesting. Notably, it has been reported that an optimal AgNP loading of approximately 3 wt% yields the most significant improvement, whereas exceeding this threshold leads to a deterioration in piezoelectric properties due to a reduced effective polarization voltage. Accordingly, the AgNP content in this work was set with reference to this optimized loading level. Fibrous piezoelectric sensing materials exhibit significant advantages over traditional film materials due to their unique one-dimensional (1D) structure.[25] They meet the core requirements of wearable smart materials, including comfort, durability, and multifunctionality, and have thus emerged as a research focus in fields such as smart apparel, wearable health monitoring, and motion sensing.[26–28] The main preparation technologies can be categorized into three types: electrospinning, melt spinning, and wet spinning. Electrospinning realizes fiber formation from spinning dope driven by a high-voltage electric field, enabling the fabrication of nanoscale fibers. Although its porous structure is conducive to breathability, the resulting fibrous materials exhibit extremely low mechanical strength (typically <10 MPa in breaking strength), and the production efficiency of a single nozzle is only 0.1–1 g h^{-1}, which limits its wide application.[29,30] Melt spinning achieves fiber formation *via* high-temperature melting of polymers. While it possesses industrial-scale mass production capability, the high-viscosity molten polymers lead to poor dispersion of inorganic particles and limited powder loading (<30%). Additionally, the high-temperature processing environment causes deterioration of PZT's piezoelectric performance.[31,32] In contrast, wet spinning is a continuous fiber production process involving solution extrusion followed by coagulation bath solidification. It offers greater room for regulating particle dispersion in the spinning dope, enabling continuous spinning of fibers with high powder loading.[33–35] Meanwhile, its processing temperature is close to room temperature, which avoids performance degradation of functional fillers caused by high temperatures.

Nonetheless, high functional filler loadings tend to induce filler agglomeration and interface defects due to the significant polarity difference between the organic polymer matrix and the inorganic fillers and insufficient interfacial bonding force, resulting in a decrease in performance and significant damage to mechanical properties. For instance, it has been well documented in wet-spun functional fibers that inorganic filler loadings exceeding 60 wt% typically result in an elongation at break below 200%.[36–38] These literature values highlight the persistent challenge of simultaneously achieving high filler content and retaining mechanical flexibility in polymer composite fibers. Concurrently, the voids hinder the interfacial transport of piezoelectric charges, ultimately leading to charge dissipation. Hence surface modification is essential to address compatibility and interfacial issues.[39–41]

To address these critical challenges, this study presents a synergistic process strategy involving the integration of interface modification and *in situ* reduction. Specifically, a high-concentration PZT dispersion is first formulated *via* silane coupling agent functionalization combined with ultrasonic dispersion, followed by the introduction of a silver precursor and TPU to yield a homogeneous spinning dope. Subsequently, *in situ* reduction is implemented to convert silver ions within the dope into AgNPs, and Ag/PZT/TPU composite piezoelectric fibers are ultimately fabricated *via* wet spinning. The results demonstrate that the as-fabricated composite fibers possess superior piezoelectric sensing capabilities, robust organic–inorganic interfacial adhesion, and excellent mechanical performance (a breaking strength exceeding 10 MPa and an elongation at break of over 200%). Upon fabrication into fabrics and subsequent poling, the resultant assemblies exhibit an exceptional piezoelectric sensitivity of up to (133 ± 2.1) mV N^{-1}. This work lays a solid foundation for the advancement of wearable sensing fabrics by offering novel functional fibrous materials and valuable technical insights.

2 Experimental section

2.1 Materials

Piezoelectric ceramic (PZT, particle size: 500–1000 nm, analytical grade, Quanzhou Qijin New Materials Technology Co., Ltd); thermoplastic polyurethane (TPU, chemical grade, Shanghai Vita Chemical Reagent Co., Ltd); *N*,*N*-dimethylformamide (DMF, analytical grade, Shanghai Aladdin Biochemical Technology Co., Ltd); silver trifluoroacetate (chemical grade, Shanghai Macklin Biochemical Technology Co., Ltd); ascorbic acid (reducing agent, chemical grade, Shanghai Macklin Biochemical Technology Co., Ltd); silane coupling agent (KBM-503, chemical grade, Shin-Etsu Chemical Co., Ltd, Japan). All of the chemicals were used as received without further purification.

2.2 Preparation of spinning solution

PZT [$Pb(Zr_XTi_{1-X})O_3$] powder and silane coupling agent (KH550) were added to DMF. First, magnetic stirring was conducted at room temperature for 1 h, followed by ultrasonic dispersion (FS-1200N) in an ice-water bath for 20 min to obtain a modified PZT dispersion. TPU was then added to the dispersion, and magnetic stirring was maintained for 8 h until complete dissolution, yielding the PZT/TPU spinning dope. Meanwhile, a 25 wt% ascorbic acid solution was prepared using DMF as the solvent, serving as the reducing agent for later use. Subsequently, silver trifluoroacetate powder was added to the PZT/TPU spinning dope, and the mixture was stirred for 2 h until the powder was completely dissolved and thoroughly mixed with the dope, with the entire process protected from light. Finally, the prepared reducing agent was dropwise added to the aforementioned spinning dope, and continuous stirring was performed for 1 h to ensure sufficient *in situ* reduction of Ag^+ to AgNPs, thus obtaining the Ag/PZT/TPU spinning dope. The reaction formula is shown below:

$$2AgOCOCF_3 + C_6H_8O_6 \rightarrow 2Ag(s) + C_6H_6O_6 + 2CF_3COOH$$

The reduction process is initiated by deprotonation of ascorbic acid, yielding a monoanion that transiently coordinates with Ag. This coordination event triggers electron transfer, leading to the oxidation of ascorbate to dehydroascorbic acid and the simultaneous reduction of surrounding Ag^+ to Ag^0. The resultant Ag^0 undergo rapid nucleation and isotropic growth, yielding colloidal nanoparticles. The trifluoroacetate counterions, acting as weakly coordinating anions, remain spectator species throughout the reduction and are ultimately protonated to release trifluoroacetic acid without perturbing the nucleation kinetics. Compared with the commonly employed nitrate counterpart, silver trifluoroacetate exhibits superior solubility in organic media and suppressed side reactions, enabling the formation of smaller and more uniformly dispersed Ag nanoparticles with homogeneous distribution within the spinning dope (Fig. 1).

2.3 Wet-spinning process

Prior to spinning, the Ag/PZT/TPU spinning dope was allowed to stand statically in a vacuum oven (YK-A1, ≤0.08 MPa) for 30 min to remove trapped air bubbles *via* degassing. Wet spinning was performed using a 21G spinning nozzle, and the spinning dope was injected into a coagulation bath consisting of hot water (80–85 °C). As the solvent in the spinning dope continuously diffused and precipitated, the as-spun fibers solidified and formed. Subsequently, the as-spun fibers, following drawing by the drawing rollers, were collected by the winding device, thus yielding continuous Ag/PZT/TPU fibers. The diameter of the fibers was controlled by adjusting the injection rate, the rotation speed of the first drawing roller, and the drawing ratio. In this study, the injection rate was set at 2 mm min^{-1}, that of the first drawing roller was 8.5 rpm, and the drawing ratio was 1.5. Afterward, the as-spun Ag/PZT/TPU fibers were fully dried in an oven at 50 °C for 1 h. According to the different filler contents, the prepared fiber samples were named Ag_xPZT_y/TPU, where x denotes the mass fraction of AgNPs and y represents the mass fraction of PZT. For example, Ag_3PZT_{80}/TPU denotes the theoretical loading of 3 wt% AgNPs and 80 wt% PZT fillers incorporated into the TPU matrix, respectively.

2.4 Preparation of the fiber-based wearable sensor

Fiber-based wearable sensors were fabricated *via* weaving and polarization treatment of Ag/PZT/TPU fibers. A portion of the fibers was sequentially threaded through healds and fixed onto a warp beam to form warp yarns, while the other portion was wound around shuttles to obtain weft yarns. The composite fibers were woven into plain-woven fabrics using a sample loom. Subsequently, the fabrics were fixed in an film corona polarization instrument for polarization treatment (FCP, BALAB), with the following parameters set: grid voltage of 10 kV, corona onset voltage of 15 kV, and treatment time of 1 h. During the treatment, the sample stage performed reciprocating motion at a moving speed of 8 mm s^{-1}. Under the action of the high-voltage electric field, the domains of PZT particles oriented along the electric field direction, transforming the originally isotropic composite fabric into an anisotropic one and thereby endowing it with piezoelectric properties. After the completion of polarization, the piezoelectric effect-based fiber-based wearable sensors were finally obtained.

2.5 Characterization

The surface and cross-sectional morphology of Ag/PZT/TPU fibers was observed with a scanning electron microscope (SEM, Gemini SEM 300). For the observation of fiber surface morphology, the fibers were cut to suitable size and stuck on the electron microscope stage using conductive tape. Cross-sectional samples of the fibers were made by freeze-brittle fracture of the fibers immersed in liquid nitrogen and then attached to cross sectional holder. Cross-sectional morphology and elemental composition were investigated *via* SEM in combination with energy-dispersive X-ray spectroscopy (EDS) after being brittlely fractured in liquid nitrogen. Samples of all the above fibers were subjected to electron microscopy after gold spraying. Tensile properties were tested by means of a single column electronic universal testing machine (EZ-LX, Shimadzu) equipped with a 10 N load cell following the general principles of ASTM D3822. Specifically, the single fiber was maintained straight and secured at both ends to the fixture of the testing machine, ensuring that the fiber axis was aligned with the loading direction, with a gauge length of 20 mm. All tests were carried out at a crosshead speed of 10 mm min^{-1} under ambient conditions (25 °C, 55% RH). At least 20 effective specimens were tested for each sample group to account for the statistical nature of fiber strength. The average breaking strength, breaking strength, and elongation at break were calculated. A certain mass of fibers was weighed for thermogravimetric (TG) experiments (STA 449 F3, NETZSCH), and the test conditions were N_2 environment with a temperature rise rate of 10 °C min^{-1} and a temperature rise interval of 40 °C to

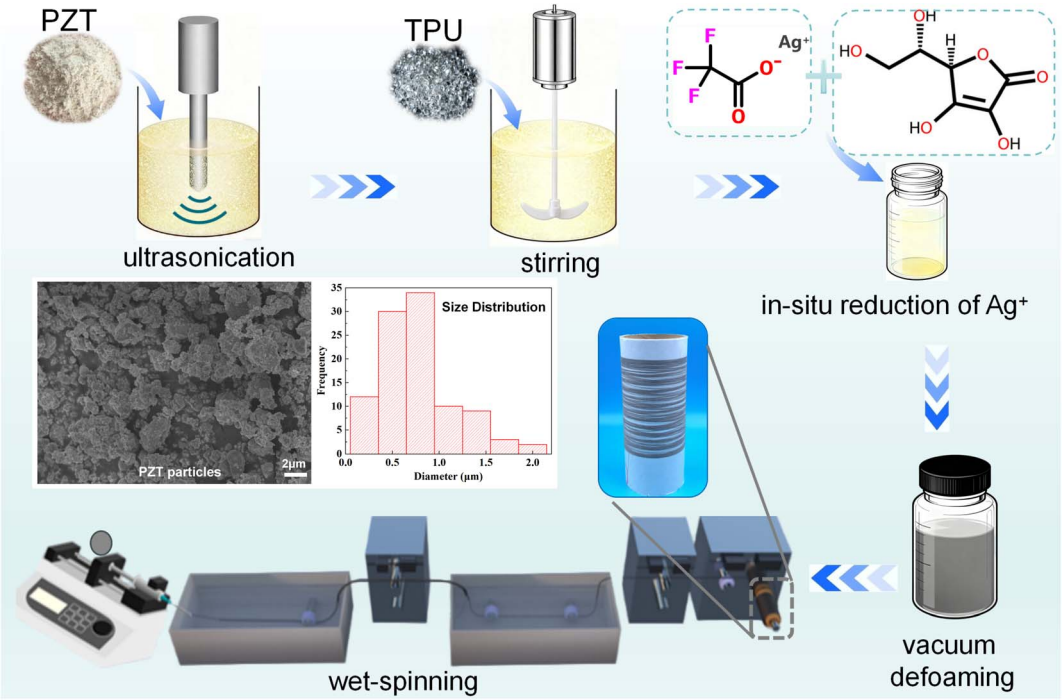

Fig. 1 Schematic diagram of the wet-spinning preparation process for PZT/TPU piezoelectric sensing fibers.

700 °C. Based on the TG test results, the actual content (W) of inorganic fillers in the composite fibers can be calculated using eqn (1):

$$W_{Ag} = \frac{W_1 - W_2}{1 - W_2} \quad (1)$$

where W_1 denotes the residue content of the composite fibers; W_2 represents the residue content of pure TPU; and W is the actual loading of inorganic fillers in the composite fibers. X-ray diffraction (XRD, D8 Discover, Bruker) was used to characterize the crystal structures of different types of composite fibers over a 2θ range of 5° to 90°. The piezoelectric properties were studied using a homemade measurement system. A load of a specific magnitude and frequency was applied using an excitation platform. The piezoelectric signals were measured with a digital storage oscilloscope (DSOX2004A, Keysight Technologies).

3 Results and discussion

3.1 Morphology of Ag/PZT/TPU fibers

Fig. 2(a) and (b) illustrate the overall morphology and microstructure of the surface and cross-section of Ag/PZT/TPU fibers, respectively. It can be observed from the figures that the fibers exhibit an overall cylindrical shape with irregular grooves on the surface and fine micropores in the interior. A large number of PZT and AgNPs are uniformly dispersed inside the fibers without obvious particle agglomeration, indicating that the "two-step method" combining ultrasonic dispersion and *in situ* reduction can effectively avoid the uneven dispersion issue in the system caused by the addition of a large amount of inorganic materials.

The formation mechanism of such a microstructure in the fibers is as follows: during the wet spinning process, after the spinning dope jet enters the coagulation bath, the surface first solidifies through the double diffusion of solvent and coagulant, while the solidification of the core layer lags behind that of the skin layer.[42,43] This lag becomes more pronounced when a large number of inorganic particles are present in the system.[44] At this point, the shaped skin layer is subjected to uneven stress induced by the shrinkage of the core layer, leading to the formation of grooves on the fiber surface. Meanwhile, micropores are formed inside the fibers as the solvent in the core layer precipitates. The presence of micropores can further enhance the flexibility of the TPU based fibers. However, if the micropores occur at the interface between PZT and TPU, they will exert an adverse effect on the piezoelectric properties of the fibers.[35]

Due to the poor compatibility between PZT and TPU, direct addition of PZT to prepare the spinning dope for wet spinning tends to result in uneven dispersion of PZT and interface defects between PZT and the TPU matrix, as shown in Fig. 3(a). These defects manifest as visible gaps, debonded zones, and insufficient contact areas at the PZT-TPU interface, as evidenced by SEM. This interfacial morphology originates from the intrinsic physicochemical incompatibility between the two phases. The fundamental disparity in surface energy and chemical affinity leads to insufficient thermodynamic driving force for interfacial wetting and mutual diffusion during the wet-spinning process. Moreover, the absence of chemical interactions across the phase boundary further exacerbates the interfacial instability. In contrast to thin films, the fiber structure renders post-treatment methods such as hot pressing

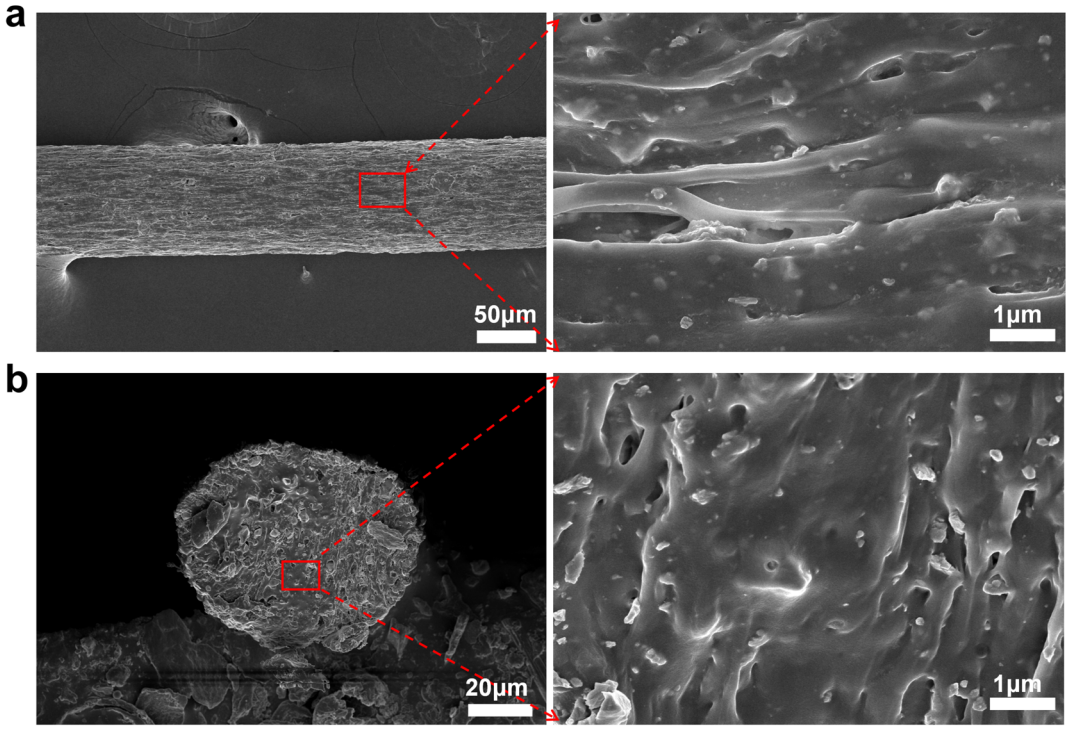

Fig. 2 SEM images of (a) surface and (b) cross-section of Ag_3PZT_{70}/TPU fibers.

inapplicable for enhancing the interfacial performance of the composite system. Therefore, it is of great significance to develop methods suitable for optimizing organic–inorganic interfaces specifically for spinning-based composite fiber fabrication. In this work, prior to preparing the spinning dope, PZT was surface-modified using a silane coupling agent. It was found that the compatibility between the silane coupling agent-modified PZT and the matrix was significantly improved. The alkoxysilane groups first undergo hydrolysis to generate reactive silanol groups, which subsequently condense with hydroxyl species present on the hydrated PZT surface, forming robust covalent M–O–Si bonds instead of M–O–M. This chemically anchors the silane onto the ceramic filler. Concurrently, amine moieties react readily with isocyanate groups (–NCO) from the TPU prepolymer or chain extender, yielding urea linkages that integrate the silane-modified PZT into the polymer matrix. The establishment of a durable interphase, critical for enhancing stress transfer efficiency and mitigating interfacial debonding, is achieved *via* a dual covalent bonding strategy. As shown in Fig. 3(b), PZT particles were tightly encapsulated within the TPU polymer matrix, and no obvious gaps existed between the two phases. This indicates that pre-treatment of PZT with a silane coupling agent is highly necessary, as it can effectively address the issues of poor mechanical and piezoelectric properties of composite fibers caused by interface defects.

3.2 Composition and phase analysis of Ag/PZT/TPU fibers

Coupled with SEM images, EDS was employed to conduct microscopic elemental distribution and content analysis on the cross-section of the composite fibers. As illustrated in the

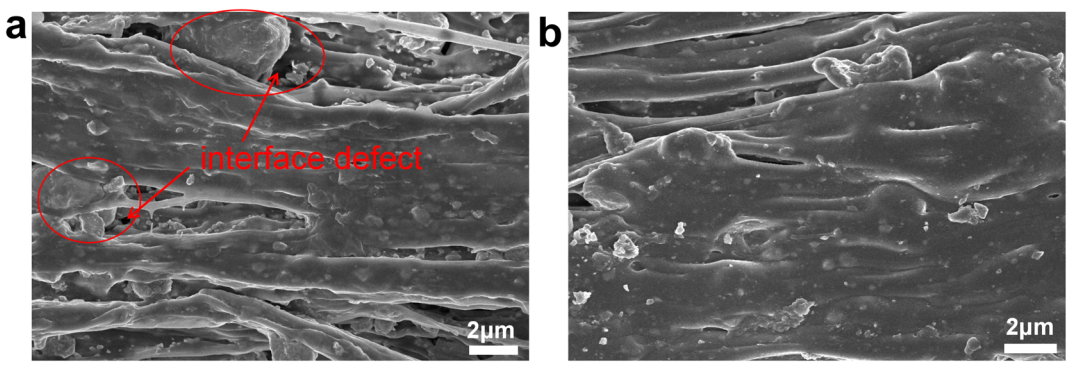

Fig. 3 SEM images of the fibers compound with (a) untreated PZT and (b) silane coupling agent-treated PZT.

elemental mapping images in Fig. 4(a), both PZT and Ag exhibit excellent dispersibility within the fibers, with no obvious agglomeration observed. This indicates that ultrasonic dispersion and *in situ* reduction strategies enable the homogeneous dispersion of high-content inorganic phases (PZT and Ag) within the fiber matrix, which is beneficial to the mechanical and piezoelectric properties of the composite fibers.

From the EDS line scan spectrum in Fig. 4(b), the metallic elements in the fibers primarily consist of Pb, Zr, Ti, and Ag. Among these, the first three are the primary constituent elements of PZT, with weight percentages of 71.24 wt%, 15.94 wt%, and 8.16 wt% respectively, corresponding to an atomic ratio of approximately 2 : 1 : 1. This ratio is consistent with the stoichiometric ratio of Pb to (Zr + Ti) in the perovskite structure of $Pb(Zr,Ti)O_3$.[45] The Ag element in the composite fibers comprises both AgNPs, which were *in situ* reduced in the spinning dope, and a residual fraction of unreduced Ag^+, with the total Ag mass fraction accounting for 4.66 wt% of the overall metal content. The slight discrepancy between the measured Ag content and the initial loading is attributed to the migration of a portion of Ag^+ into the coagulation bath during wet spinning. Based on the stoichiometry of the perovskite $Pb(Zr,Ti)O_3$ phase

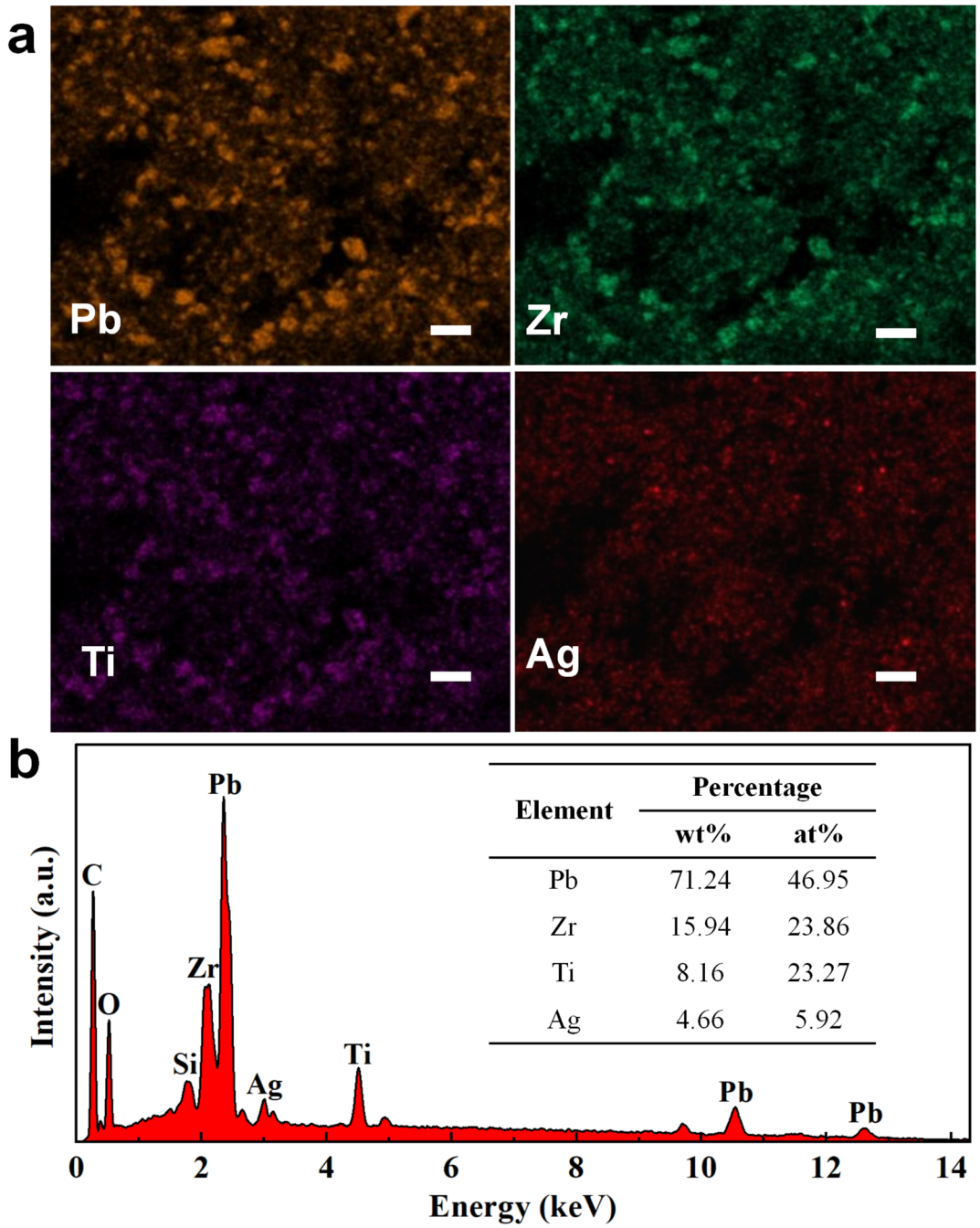

Element	Percentage	
	wt%	at%
Pb	71.24	46.95
Zr	15.94	23.86
Ti	8.16	23.27
Ag	4.66	5.92

Fig. 4 Elemental mapping images (a) and corresponding EDS spectra of the Ag_3PZT_{70}/TPU fiber cross-sections (b).

and the mass of the polymer matrix, the mass fraction of AgNPs in the final composite fibers is calculated to be approximately 2.84 wt% relative to the total composite mass. In addition, trace amounts of Si element were detected, which is mainly derived from KH550.

Subsequently, further analysis was conducted on the inorganic content and phase structure of the fibers. It can be observed from Fig. 5(a) that the TG curves of different fibers exhibit a three-stage continuous weight loss behavior, consistent with the thermal decomposition trend of pure TPU fibers. This is attributed to the fact that TPU molecular chains consist of soft segments and hard segments, which exhibit significant differences in decomposition temperatures. The mass retention rates of pure TPU, PZT/TPU composite fibers, and composite fibers at 700 °C are 5.01%, 71.20%, and 73.27%, respectively. It can be calculated, using eqn (1), that the actual loadings of PZT and Ag in the composite fibers are 69.68% and 2.18%, respectively. The Ag content is slightly lower than the value calculated from the EDS. Slight variations in the actual stoichiometry of the PZT phase from the ideal perovskite model, coupled with trace residues from polymer pyrolysis during TG measurement, may also account for the observed discrepancy. Furthermore, the initial decomposition temperature of PZT/TPU composite fibers is lower than that of pure TPU, which is presumably caused by the decomposition of trace small-molecule modifiers in the composite fibers.[46] After the introduction of AgNPs, the nucleation effect of AgNPs improves the thermal resistance of the composite fibers to a certain extent at the initial stage of heating.[47]

As shown in Fig. 5(b), XRD pattern of pure TPU fibers exhibits no distinct crystalline diffraction peaks, but rather a broad, weak amorphous scattering signal with a dominant broad diffraction peak centered at 20.2°. This is characteristic of the crystallization region of polymers. After incorporating PZT into the TPU matrix, the composite fibers show diffraction peaks at $2\theta = 31.1°$, 31.6°, and 44.4°, which correspond to the rhombohedral phase of $Pb(Zr,Ti)O_3$ (JCPDS card no. 73-2022). The weak characteristic peak at $2\theta = 21.8°$ is presumably attributed to PbO impurities formed during PZT synthesis.[48] Since the piezoelectric properties of the composite fibers are primarily derived from the unique crystalline structure of PZT, this result confirms that the piezoelectric functionality of PZT remains intact after wet-spinning process. After being incorporated with Ag^+, in addition to the characteristic peaks of TPU and PZT (consistent with the above observations), extra crystalline diffraction peaks at $2\theta = 38.3°$, 44.3°, 64.5°, and 77.5°, which could be assigned to the crystal planes (111), (200), (220) and (311) of the face-centered cubic structure of AgNPs, respectively. This confirms the successful reduction of the added Ag^+ to AgNPs.[49] With respect to the TPU matrix, after the introduction of PZT and Ag, the position of its diffraction peak remains unchanged; however, the peak intensity decreases and the full width at half maximum increases, indicating that the presence of these inorganic phases exerts a certain influence on both the crystallinity and crystalline order of the TPU based fibers.

3.3 Mechanical properties of Ag/PZT/TPU fibers

Fig. 6 presents the stress–strain curves of Ag/PZT/TPU composite fibers with varying Ag and PZT loadings, where Fig. 6(a) illustrates the effect of Ag content on the tensile mechanical properties of the TPU matrix. As observed from the figure, with an increase in Ag content, the elongation at break of the fibers exhibits a significant decrease, while the breaking strength first slightly increases followed by a subsequent decline. This phenomenon indicates that the AgNPs, obtained *via in situ* reduction, are uniformly dispersed within the TPU matrix. Specifically, the nanoparticles restrict the mobility of polymer molecular chains in the matrix, thereby reducing the deformability of the fibers. Concurrently, they confer a certain degree of reinforcement effect through mechanisms such as stress transfer and interfacial interactions. However, at excessive Ag contents, the nanoparticles tend to agglomerate. Consequently, stress concentration tends to arise around these agglomerates, which in turn accelerates the initiation and propagation of cracks, ultimately resulting in a reduction in

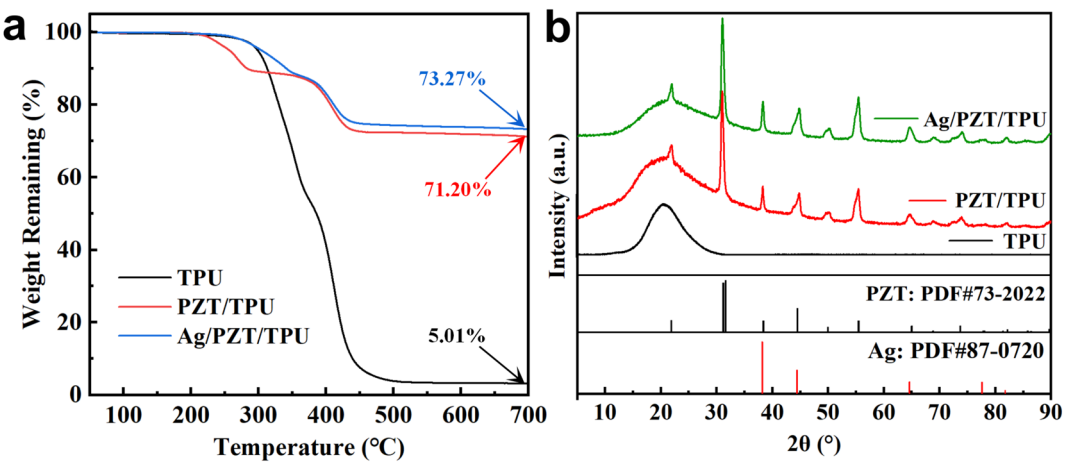

Fig. 5 TGA curves (a) and XRD patterns (b) of different Ag_3PZT_{70}/TPU composite fiber samples.

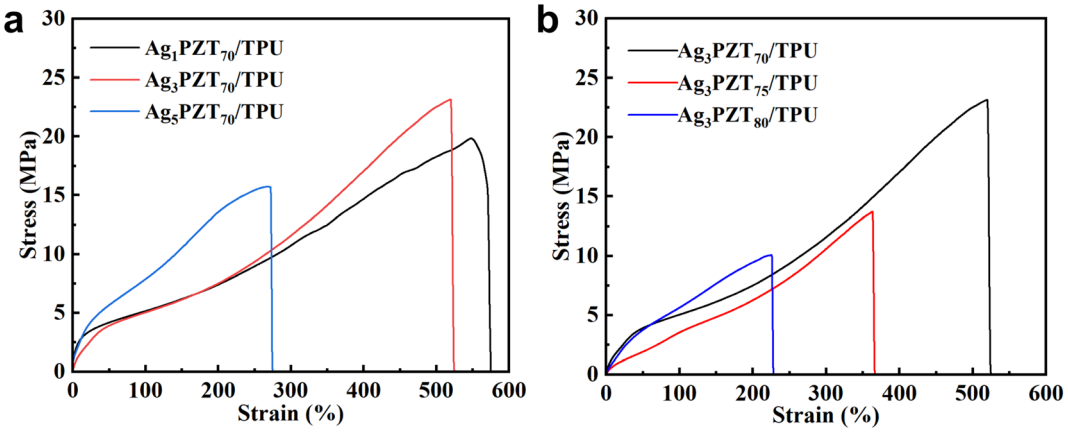

Fig. 6 Stress–strain curves of different Ag/PZT/TPU composite fibers: (a) varying Ag contents; (b) varying PZT contents.

breaking strength during tensile deformation of the composite fibers. Thus, the Ag content must be controlled within a reasonable range to avoid the deterioration of the fiber's mechanical properties and even achieve a moderate reinforcement effect.

Fig. 6(b) focuses on the effect of PZT loading on the tensile mechanical properties of the composite fibers. As observed from the figure, the Ag_3PZT_{70}/TPU sample exhibits the highest tensile strength (23.1 MPa) and elongation at break (520%). With the increase in PZT loading, both the tensile strength and elongation at break of the fibers decrease. Notably, when the loading of the piezoelectric ceramic filler PZT reaches as high as 80 wt% with the simultaneous incorporation of Ag particles, the prepared composite fibers still maintain an elongation at break of over 200%. These composite fibers didn't exhibit brittleness, easy fracture, or other issues caused by high inorganic filler content, retaining comprehensive processability including cutting, weaving, and bending capabilities. This indicates that wet spinning is an efficient and reliable method for preparing high-quality composite fibers with high inorganic filler loadings, which also lays a solid foundation for the application of such fibers in flexible electronics, wearable devices, and other scenarios.

3.4 Piezoelectric performance of Ag/PZT/TPU fibers

As shown in Fig. 3(a), the preparation of the piezoelectric fabric sensor requires additional processing steps, which involves coating the outer piezoelectric layer with copper foil tape. A piezoelectric sensing structure was then established, where macroscopic accumulation of polarized charges formed in the fabric layer due to the piezoelectric effect.

The effect of the mass ratio of PZT and Ag to TPU on the sensitivity of composite fibers was investigated, as presented in Fig. 7(b). As a key filler conferring piezoelectric properties, it exhibits a prominent concentration-dependent trend in enhancing the piezoelectric performance of piezoelectric fabrics. Specifically, within the low concentration range (60–80 wt%), the piezoelectric performance of the fabrics is prominently enhanced with increasing AgNPs concentration. When the concentration approaches the percolation threshold, the performance attains a maximum of (133 ± 2.1) mV N^{-1} at a PZT mass ratio of 80 wt%, whereas a further increase in content conversely results in a decline in performance.

The initial enhancement of sensitivity with the increasing PZT proportion can be attributed to the increased number of piezoelectric domains provided by the PZT filler, which is a factor that dictates the total amount of charge separation and generation when the fabrics are subjected to stress. Meanwhile, under this condition, PZT forms a homogeneous distribution of the active phase inside the fibers, and a robust interface is formed between the PZT particles and TPU matrix. This facilitates the efficient transmission of external mechanical excitation to the interior of PZT, thereby inducing the oriented deflection and polarization of piezoelectric domains.[22,41] However, an excessive PZT content may compromise the sensitivity, primarily due to particle aggregation, impaired fiber formability and interfacial bonding failure during wet spinning. In this case, some PZT piezoelectric domains fail to undergo sufficient polarization; simultaneously, the increased interfacial defects exacerbate charge dissipation. Ultimately, this compromises the electromechanical conversion efficiency of the piezoelectric fibers, ultimately leading to degraded sensing and mechanical properties.[50]

As for Ag, within the low-content regime, the piezoelectric properties of the fabric improve as the Ag precursor reaches 3 wt% (approaching the percolation threshold), the performance achieves the optimal level, and further increases in content result in a subsequent decline. The fundamental mechanisms can be primarily categorized into three aspects:[51–53] (1) the excellent electro-conductivity of Ag NPs serves to reduce the leakage loss of the composite fiber and facilitates the oriented alignment of electric domains within the piezoelectric phase during polarization, thereby enhances the polarization efficiency of the fabric; (2) the synergistic filling of micro–nano scale fillers enables the construction of more efficient stress transfer pathways, thereby facilitating the more effective conversion of external mechanical forces into electrical signals. More efficiently converted into the deformation and

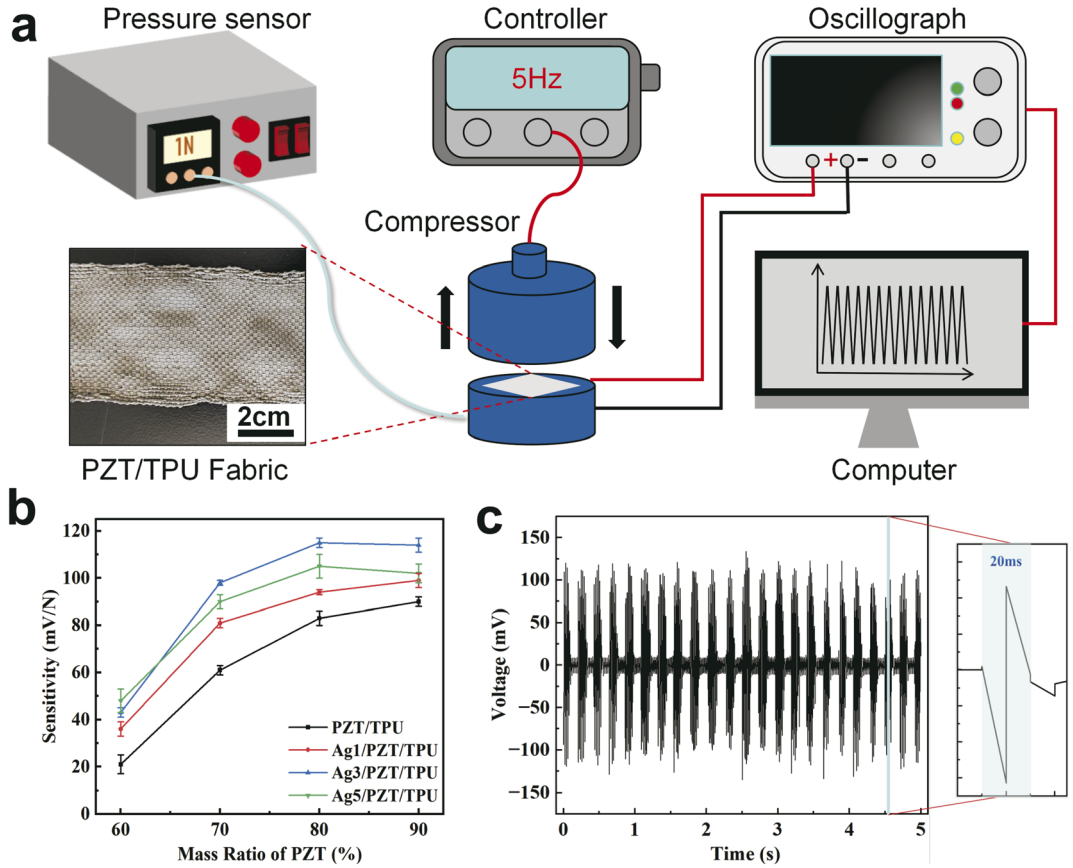

Fig. 7 Piezoelectric performance evaluation of Ag/PZT/TPU fibers. (a) Schematics of the piezoelectric fabric with copper electrode and the setup used to measure its piezoelectric signal. (b) Piezoelectric sensing performance of fibers with different PZT and Ag contents; (c) piezoelectric sensing performance of fibers under the pressure of 5 Hz and 1 N.

charge separation of the piezoelectric phase; (3) the discrete and uniformly distributed conductive nano-silver form localized conductive sites, which can efficiently capture and conduct the free charges generated by the piezoelectric effect, reduce charge recombination and leakage losses, and thereby enhance the electromechanical conversion efficiency of the composite material.

Overall, when the loading content of the silver precursor is 3% and that of PZT is 80%, the piezoelectric sensing performance of the piezoelectric composite fibers attains the optimal level. Under this optimal ratio condition, the synergistic effect of the binary fillers system achieves a synergistic enhancement effect on the improvement of the piezoelectric properties of the fibers, significantly enhancing the electromechanical conversion efficiency of the material and laying a critical performance foundation for its sensing applications.

Fig. 7(c) shows the piezoelectric sensing performance of the piezoelectric fabric under the test conditions of a frequency of 5 Hz and an applied pressure of 1 N. Specifically, the peak output voltage of the fabric can reach 135 mV, which enables it to effectively respond to low-load mechanical stimuli and exhibits a robust signal output capability. Collectively, the aforementioned output voltage characteristics demonstrate that the material possesses reliable signal capture and output capabilities in low-frequency, low-load sensing scenarios, thereby providing core performance support for subsequent sensing applications. The inset of Fig. 7(c) reveals the rapid response characteristics of the sensor fabric, which exhibit a response time as short as 20 ms to instantaneous loads, indicating its excellent capability in capturing transient events.

4 Conclusions

Ag/PZT/TPU composite fibers with exceptional mechanical and piezoelectric properties were successfully fabricated *via* wet-spinning by effectively combining surface modification and *in situ* reduction techniques. Owing to the excellent dispersion of fillers in the fiber matrix, the breaking strength and elongation at break of the fibers remain above 10 MPa and 200%, respectively, even at a filler loading of over 80 wt%. When the PZT content in the Ag/PZT/TPU fibers is 80 wt% and the Ag precursor content is 3 wt%, the fiber-based wearable sensor delivers the optimal piezoelectric sensing performance, with an output voltage of (133 ± 2.1) mV N^{-1}. Overall, the as-prepared Ag/PZT/TPU fibers hold great promise for advancing sensor technology and flexible electronics, along with substantial potential in smart textile materials.

Author contributions

Wanwan Liu: writing-original draft, writing-review & editing, visualization, validation, project administration, methodology, investigation, formal analysis, data curation, resources, conceptualization. Huabin Li: writing-review & editing, investigation, data curation, formal analysis, validation. Jingjing Xu: writing-review & editing, validation, data curation, methodology. Shuangquan Wu: writing-review & editing, project administration, validation, methodology. Zhidong Chen: writing-review & editing, conceptualization, supervision, funding acquisition, project administration.

Conflicts of interest

The authors declare no conflict of interest.

Data availability

The data that support the findings of this study are available from the corresponding author upon reasonable request.

Acknowledgements

The authors gratefully acknowledge the financial support from "Pioneer" and "Leading Goose" Research and Development Program of Zhejiang (No. 2022C01166) and Changzhou Science and Technology Program (CJ20250004).

References

1 Z. Song, R. Hou and F. Jiang, Recent progress in piezoelectric thin films as self-powered devices: material and application, *Front. Mater.*, 2024, **11**, 1–18, DOI: 10.3389/fmats.2024.1373040.

2 Y. Zhong, Y. Wang, L. Ma, P. He, J. Qin, J. Gao and J. Li, Ultrasensitive piezoelectric sensor based on polyimide foam for sound recognition and motion monitoring, *ACS Appl. Mater. Interfaces*, 2025, **17**, 11154–11163, DOI: 10.1021/acsami.4c22301.

3 X. Cao, Y. Xiong, J. Sun, X. Zhu, Q. Sun and Z. Wang, Piezoelectric nanogenerators derived self-powered sensors for multifunctional applications and artificial intelligence, *Adv. Funct. Mater.*, 2021, **31**, 2102983, DOI: 10.1002/adfm.202102983.

4 X. Liu, Y. Wang, W. Wang, M. Cheng, A. Yu, L. Wan and J. Zhai, Humidity-resistant, breathable, waterproof, and bionic triboelectric electronic skins for self-powered haptic sensing and human motion recognition, *Chem. Eng. J.*, 2024, **490**, 151771, DOI: 10.1016/j.cej.2024.151771.

5 H. Kil and J. Park, Carotid artery monitoring patch using a supercapacitive pressure sensor with piezoelectricity, *Nano Energy*, 2023, **114**, 108636, DOI: 10.1016/j.nanoen.2023.108636.

6 S. Wei and T. Ghosh, Moisture-driven cellulose actuators with directional motion and programmable shapes, *Adv. Intell. Syst.*, 2024, **6**, 2300638, DOI: 10.1002/aisy.202300638.

7 M. Li, L. Wu, G. Zheng, X. Zhang, Z. Liang, M. Liu, R. Li, J. Zhang and Y. Long, Flexible piezoelectric-thermoelectric coupled nanofiber generator for self-powered multimodal sensing system, *Adv. Funct. Mater.*, 2025, e16438, DOI: 10.1002/adfm.202516438.

8 R. Hou, L. Xu, M. Yu, Z. Tang, B. Zhou, Q. Zhang, N. Li and J. Xu, Piezoelectric-triboelectric hybrid nanogenerator based on tough, stretchable $BaTiO_3$ doped antibacterial hydrogel for self-powered sensors, *Supramol. Mater.*, 2025, **4**, 100096, DOI: 10.1016/j.supmat.2025.100096.

9 W. Chen, S. Liu, J. Zhuang, D. Zhang, X. Tang, V. Roy and Q. Sun, Emerging metal oxide based triboelectric nanogenerators for energy collection and self-powered sensing, *Mater. Sci. Eng., R*, 2026, **167**, 101119, DOI: 10.1016/j.mser.2025.101119.

10 M. Zarei, A. Jeong and S. Lee, Whisker-implanted biomimetic electronic skin for tactile sensing and blind perception, *Adv. Sci.*, 2025, **12**, 2408162, DOI: 10.1002/advs.202408162.

11 L. Gong, T. Xuan, S. Wang, H. Du and W. Li, Liquid metal based triboelectric nanogenerator with excellent electrothermal and safeguarding performance towards intelligent plaster, *Nano Energy*, 2023, **109**, 108280, DOI: 10.1016/j.nanoen.2023.108280.

12 B. Chen, H. Li, W. Tian and C. Zhou, PZT based piezoelectric sensor for structural monitoring, *J. Electron. Mater.*, 2019, **48**, 2916–2923, DOI: 10.1007/s11664-019-07034-8.

13 T. Zhao, J. Li, X. Yang and Z. Yin, A review of the preparation and application of lead zirconate titanate (PZT) thin film sensors, *J. Mater. Chem. C*, 2025, **13**, 15807–15851, DOI: 10.1039/d5tc01573a.

14 B. Qin, G. Ding, X. Yang, W. Li, Y. He, A. Ren, W. Xing, S. Tan, X. Wei and Z. Zhang, Ultrahigh piezoelectric coefficients achieved by tailoring the sequence and nano-domain structure of P(VDF-TrFE), *Adv. Mater.*, 2025, **37**, 2502708, DOI: 10.1002/adma.202502708.

15 M. Li, L. Wu, G. Zheng, X. Zhang, Z. Liang, M. Liu, R. Li, J. Zhang and Y. Long, Flexible piezoelectric-thermoelectric coupled nanofiber generator for self-powered multimodal sensing system, *Adv. Funct. Mater.*, 2025, e16438, DOI: 10.1002/adfm.202516438.

16 Y. Li, S. Zhang, H. Gu, Y. Li, H. Zhao, S. Huang, X. Feng, C. Zhai and M. Xu, Ultrasensitive piezoelectric-like film with designed cross-scale pores, *Sci. Adv.*, 2025, **11**, eadt4003, DOI: 10.1126/sciadv.adt4003.

17 J. Fan, R. Yang, Y. Du, F. Wang, L. Wang, J. Yang and A. Zhou, A triboelectric nanogenerator based on MXene/TPU composite films with excellent stretchability for self-powered flexible sensing, *Nano Energy*, 2024, **129**, 109999, DOI: 10.1016/j.nanoen.2024.109999.

18 Y. Wang, B. Yan, Y. Zhou, G. Zhao, Q. Liu, H. Liu, Z. Lin, X. Peng and T. Chen, Hierarchical porous TPU@CNT sponge for high-performance triboelectric nanogenerators via dual contact electrification and self-powered sensing applications, *Chem. Eng. J.*, 2025, **521**, 166530, DOI: 10.1016/j.cej.2025.166530.

19 Q. Yuan, Z. Gao, K. Xia, M. Weng, Z. Huang, R. Liu, T. Wu and J. Qu, Scalable fabrication of bioinspired flexible sensor with gradient modulus and conductivity for intelligent gait recognition, *Adv. Funct. Mater.*, 2025, e12249, DOI: 10.1002/adfm.202512249.
20 T. Lucas, E. Moiseeva, G. Zhang, A. Gobin and C. Harnett, Thermal properties of infrared absorbent gold nanoparticle coatings for MEMS applications, *Sens. Actuators, A*, 2013, **198**, 81–86, DOI: 10.1016/j.sna.2013.04.033.
21 M. Habib, I. Lantgios and K. Hornbostel, A review of ceramic, polymer and composite piezoelectric materials, *J. Phys. D: Appl. Phys.*, 2022, **55**, 423002, DOI: 10.1088/1361-6463/ac8687.
22 H. Chen, W. Liu, H. Xia, Y. Qiu, Q. Ni and Y. Fu, Flexible nanopositioning actuators based on functional nanocomposites, *Compos. Sci. Technol.*, 2020, **186**, 107937, DOI: 10.1016/j.compscitech.2019.107937.
23 Z. Zhou, Z. Zhang, Q. Zhang, H. Yang, Y. Zhu, Y. Wang and L. Chen, Controllable core-shell $BaTiO_3$@Carbon nanoparticle-enabled P(VDF-TrFE) composites: a cost-effective approach to high-performance piezoelectric nanogenerators, *ACS Appl. Mater. Interfaces*, 2020, **12**, 1567–1576, DOI: 10.1021/acsami.9b18780.
24 B. Liu, X. Zhang, B. Li and X. Zhang, Interfacial dielectric enhancement in MXene/PVDF nanocomposites via hydrogen bond-induced dipole modulation, *Appl. Surf. Sci.*, 2025, **695**, 162837, DOI: 10.1016/j.apsusc.2025.162837.
25 Y. Chen, X. Zhangb and C. Lu, Flexible piezoelectric materials and strain sensors for wearable electronics and artificial intelligence applications, *Chem. Sci.*, 2024, **15**, 16436, DOI: 10.1039/d4sc05166a.
26 Y. Yang, Y. Liu and R. Yin, Fiber/yarn and textile-based piezoresistive pressure sensors, *Adv. Fiber Mater.*, 2025, **7**, 34–71, DOI: 10.1007/s42765-024-00479-5.
27 W. Lu, G. Wu, L. Gan, Y. Zhang and K. Li, Functional fibers/textiles for smart sensing devices and applications in personal healthcare systems, *Anal. Methods*, 2024, **16**, 5372–5390, DOI: 10.1039/d4ay01127a.
28 K. Dong, X. Peng and Z. Wang, Fiber/fabric-based piezoelectric and triboelectric nanogenerators for flexible/stretchable and wearable electronics and artificial intelligence, *Adv. Mater.*, 2020, **32**, 1902549, DOI: 10.1002/adma.201902549.
29 B. Li, F. Zhang, S. Guan, J. Zheng and C. Xu, Wearable piezoelectric device assembled by one-step continuous electrospinning, *J. Mater. Chem. C*, 2016, **4**, 6988–6995, DOI: 10.1039/c6tc01696k.
30 C. Zhi, S. Shi, Y. Si, B. Fei, H. Huang and J. Hu, Recent progress of wearable piezoelectric pressure sensors based on nanofibers, yarns, and their fabrics via electrospinning, *Adv. Mater. Technol.*, 2023, **8**, 2201161, DOI: 10.1002/admt.202201161.
31 R. Schönlein, M. Fernández, I. Calafel, M. Azkune, G. Liu, A. Müller, J. Ugartemendia and R. Aguirresarobe, Flow-induced crystallization of piezoelectric poly(L-lactide) fibers by a one-step melt-spinning process, *Mater. Des.*, 2024, **237**, 112525, DOI: 10.1016/j.matdes.2023.112525.
32 H. Oh, D. Kim, Y. Choi, S. Lim, J. Jeong, J. Ko, W. Hahm, S. Kim, Y. Lee, H. Kim and B. Yeang, Fabrication of piezoelectric poly(L-lactic acid)/$BaTiO_3$ fibre by the melt-spinning process, *Sci. Rep.*, 2020, **10**, 16339, DOI: 10.1038/s41598-020-73261-3.
33 L. Pan, Y. Wang, Q. Jin, D. Wu, L. Zhu, Z. Zhou and M. Zhu, Scalable wet-spinning multilevel anisotropic structured PVDF fibers enhanced with cellulose nanocrystals-exfoliated MoS_2 for high-performance piezoelectric textiles, *Chem. Eng. J.*, 2024, **497**, 155671, DOI: 10.1016/j.cej.2024.155671.
34 X. Li, Q. Liu, Y. Liu, L. Yang, M. Li, B. Wang, Y. Li, Y. Wang, T. Wang and D. Wang, Flexible, visual, and multifunctional humidity-strain sensors based on ultra-stable perovskite luminescent filaments, *Adv. Fiber Mater.*, 2025, **7**, 762–773, DOI: 10.1007/s42765-025-00518-9.
35 W. Zhou, Z. Chen, X. Yuan, H. Yu, Y. Zhang, W. Zhao, X. Li, X. Zhang, Z. Cui, P. Fu, X. Pang and M. Liu, Self-powered wireless piezoelectric sensor based on polyamide elastomer/$BaTiO_3$ for machine learning-assisted human motion monitoring, *ACS Appl. Mater. Interfaces*, 2025, **17**, 57500–57515, DOI: 10.1021/acsami.5c12234.
36 Q. Gao, Z. Chen, C. Liu, Y. Wang, J. Zhu and C. Gao, Helical TPU/Ag@K2Ti4O9 fibers with shape memory performance for highly stretchable and sensitive strain sensors, *J. Alloys Compd.*, 2024, **980**, 173547, DOI: 10.1016/j.jallcom.2024.173547.
37 Y. Lu, J. Jiang, S. Yoon, O. Kim, J. Kim, S. Park, S. Kim and L. Piao, High-performance stretchable conductive composite fibers from surface-modified silver nanowires and thermoplastic polyurethane by wet spinning, *ACS Appl. Mater. Interfaces*, 2018, **10**(2), 2093–2104, DOI: 10.1021/acsami.7b16022.
38 J. Zhuang, Y. Liu, D. Bian, F. He, Y. Li and W. Fan, Spinning solution viscosity reducing and wet spinning of carbon black-based elastic conductive fibers for sports monitoring and healthcare electrical heating, *J. Mater. Res. Technol.*, 2025, **36**, 1–12, DOI: 10.1016/j.jmrt.2025.03.096.
39 J. Li, C. Zhao, K. Xia, X. Liu, D. Li and J. Han, Enhanced piezoelectric output of the PVDF-TrFE/ZnO flexible piezoelectric nanogenerator by surface modification, *Appl. Surf. Sci.*, 2019, **463**, 626–634, DOI: 10.1016/j.apsusc.2018.08.266.
40 S. Paria, S. Si, S. Karan, A. Das, A. Maitra, R. Bera, L. Halder, A. Bera, A. Dea and B. Khatua, A strategy to develop highly efficient TENGs through the dielectric constant, internal resistance optimization, and surface modification, *J. Mater. Chem. A*, 2019, **7**, 3979–3991, DOI: 10.1039/c8ta11229k.
41 V. Bouad, M. Girardot, V. Ladmiral and S. Barrau, Piezoelectric fluorinated polymer composites: A review on coupling agents at the filler/matrix interface, *Polym. Compos.*, 2024, **45**, 3861–3882, DOI: 10.1002/pc.28064.
42 J. White and T. Hancock, Fundamental analysis of the dynamics, mass transfer, and coagulation in wet spinning

of fibers, *J. Appl. Polym. Sci.*, 1981, **26**, 3157–3170, DOI: 10.1002/app.1981.070260928.

43 Q. Liu, H. Gao, L. Zha, Z. Hu, Y. Ma, M. Yu, L. Chen and W. Hu, Tuning bio-inspired skin-core structure of nascent fiber via interplay of polymer phase transitions, *Phys. Chem. Chem. Phys.*, 2014, **16**, 15152–15157, DOI: 10.1039/c4cp00792a.

44 B. Zhao, X. Li, C. Gu, Y. Wang, H. Liu, X. Guo, Y. Zhang, H. Tian, W. Qin and S. Yin, Highly stretchable and strain sensitive MXene/MXene: MWCNTs@TPU fiber with hierarchical conductive layers and porous elastic core structure, *Colloids Surf., A*, 2024, **690**, 133821, DOI: 10.1016/j.colsurfa.2024.133821.

45 K. Eklund and A. Karttunen, Pyroelectric properties of Pb $[Zr_{0.5}Ti_{0.5}]O_3$ studied with a hybrid density functional method, *Phys. Chem. Chem. Phys.*, 2025, **27**, 15920–15928, DOI: 10.1039/d5cp01655j.

46 A. Barick and D. Tripathy, Thermal and dynamic mechanical characterization of thermoplastic polyurethane/organoclay nanocomposites prepared by melt compounding, *Mater. Sci. Eng., A*, 2010, **527**, 812–823, DOI: 10.1016/j.msea.2009.10.063.

47 A. Manap, S. Mahalingam, R. Vaithylingam and H. Abdullah, Mechanical, thermal and morphological properties of thermoplastic polyurethane composite reinforced by multi-walled carbon nanotube and titanium dioxide hybrid fillers, *Polym. Bull.*, 2021, **78**, 5815–5832, DOI: 10.1007/s00289-020-03393-z.

48 S. Moharana, S. Joshi and R. Mahaling, Enhanced dielectric and ferroelectric properties induced by Ag@Pb(Zr,Ti)O_3 in poly(vinyl alcohol) matrix composites: A solution casting approach, *J. Appl. Polym. Sci.*, 2017, **134**, 45583, DOI: 10.1002/app.45583.

49 Q. Shi, N. Vitchuli, J. Nowak, J. Noar, J. Caldwell, F. Breidt, M. Bourham, M. McCord and X. Zhang, One-step synthesis of silver nanoparticle-filled nylon 6 nanofibers and their antibacterial properties, *J. Mater. Chem.*, 2011, **21**, 10330–10335, DOI: 10.1039/c1jm11492a.

50 H. Zhan, P. Lv, S. Zhang, L. Xin, J. Wang, R. Li, C. Li, L. Ren and M. Zhang, High-performance piezoelectric composite combined with PZT micropillars and P(VDF-TrFE) membrane for energy harvesting and sensing, *J. Alloys Compd.*, 2025, **1019**, 179227, DOI: 10.1016/j.jallcom.2025.179227.

51 Q. Xu, J. Wen and Y. Qin, Theoretical study of the stress transfer effect on the output of a composite piezoelectric nanogenerator, *ACS Mater. Lett.*, 2021, **3**, 1793–1798, DOI: 10.1021/acsmaterialslett.1c00613.

52 J. Yan, Y. Qin, M. Li, Y. Zhao, W. Kang and G. Yang, Charge-boosting strategy for wearable nanogenerators enabled by integrated piezoelectric/conductive nanofibers, *ACS Appl. Mater. Interfaces*, 2022, **14**, 55039–55050, DOI: 10.1021/acsami.2c15165.

53 C. Zhao, Y. Wang, W. Feng, T. Lin, X. Wu, M. Gao and C. Lin, High energy harvesting performance in piezoelectric composite films employing large piezoelectric fillers and interface engineering, *ACS Appl. Polym. Mater.*, 2024, **6**, 3436–3445, DOI: 10.1021/acsapm.4c00058.